



Research articles

Advanced magnetic X-ray spectro-microscopies to characterize mesoscopic magnetic materials



David Raftrey ^{a,b}, Peter Fischer ^{a,b,*}

^a Materials Sciences Division, Lawrence Berkeley National Laboratory, Berkeley, CA 94720, USA
^b Physics Department, UC Santa Cruz, Santa Cruz CA 95064, USA

ARTICLE INFO

Keywords:

Magnetic X-ray spectro-microscopy
Polarized synchrotron radiation
Spin dynamics
Topological spin textures

ABSTRACT

This article provides a brief overview of advanced magnetic X-ray spectro-microscopies that are widely used in characterizing mesoscopic magnetic materials. Common to those techniques are various X-ray magnetic dichroism effects that are used as magnetic contrast mechanism. A particular interest is to use those techniques to image the underlying microscopic spin structures in magnetic materials with high spatial resolution and to ultimately resolve their full 3D mesoscale characteristics with elemental sensitivity, as well as their ultrafast dynamics upon excitations with field and current pulses.

Recent research examples using various magnetic X-ray spectro-microscopies are presented to showcase their specific features with a focus on imaging novel topological spin textures, such as vortices, skyrmions and Hopfions, which are considered as potential building blocks towards low power, high-speed and high-density magnetic devices that could transform information technologies and potentially be used in biomedical applications.

Future developments with magnetic X-ray spectro-microscopies harness the full coherence of next generation X-ray sources and could open the path towards single shot imaging with spatial and temporal resolutions down to fundamental magnetic length and time scales.

1. Introduction

The static properties and the dynamic behavior of magnetic materials are the scientific backbone of the field of spintronics, where information and sensor technologies are built on the electronic spin instead of the electronic charge as in conventional electronics [1]. Progress in this field requires a deep understanding of the underlying physical processes, and those are generally related to the arrangement of spins into microscopic textures which result from the competition of various magnetic interactions [2]. They include short-range symmetric and antisymmetric exchange interactions, i.e., Heisenberg and Dzyaloshinskii-Moriya-type interactions [3], which in the former case favor a collinear (parallel or antiparallel) alignment of neighboring spins and a non-collinear alignment for the latter. Magnetic anisotropy energies are related to spin-orbit interactions, and dipolar interactions are the dominating long-range magnetic interactions impacting the spin textures. In addition, confinement and proximity determine the arrangement of spin structures, which has led to advanced strategies for synthesizing bespoke nanoscale magnetic materials harnessing

nanolithography techniques to create magnetic patterned nanostructures, designing interfaces in magnetic multilayered systems, and combining magnetic and non-magnetic components into complex heterogeneous magnetic systems.

Characterizing the static and dynamic characteristics of those magnetic nanostructures is key to integrating them into new technologies, but requires the development and availability of advanced characterization tools to meet the relevant **length**, **time** and **energy** scales of those magnetic materials.

The fundamental magnetic **length** scales in magnetic materials are the short-range exchange lengths, which determine the distance over which spins can change their orientation, e.g., in domain walls or vortex cores, and which are generally in the few nanometer range. The fundamental magnetic **time** scales are inversely related to the exchange energy as the strongest interaction, and reach typically into the low fs regime. Therefore, advanced magnetic microscopies target spatial and temporal resolutions on these fundamental levels. However, being able to characterize magnetic materials also across length and time scales, which responds to the size of real devices, but includes also

* Corresponding author at: Materials Sciences Division, Lawrence Berkeley National Laboratory, Berkeley, CA 94720, USA.
E-mail address: PJFischer@lbl.gov (P. Fischer).

multidimensional microscopies (tomography) and the need to investigate magnetic functionalities from the fsec to psec and nsec timescales, has become a major research direction recently. Relevant energy scales in magnetic materials are on one hand the ground state, which is often the result from synthesizing complex and multicomponent materials, including the design of interfaces, and on the other hand excited states, e.g., upon excitation with ultrafast pump pulses. The compositional and geometrical design strategies have led to elemental, chemical, and interfacial sensitivity as essential requirements in advanced magnetic spectro-microscopies to characterize mesoscopic magnetic materials.

Numerous approaches and techniques have been developed and are being used today, and they can be broadly categorized by the type of probes they are using. Those include **magneto-optical** techniques, using various MO effects, such as Kerr, Faraday, Voigt and Cotton-Mouton effects. Since the light sources in those experiments are mostly advanced optical laser systems, their strengths are in ultrafast magnetization studies down to the fsec regime [4].

Scanning probe techniques take advantage of various interactions of a sharp tip with the magnetization of the sample. Among them is Spin Polarized Scanning Tunneling Microscopy (SP-STM), which is still the leading technique in terms of having demonstrated near single-atom spatial resolution [5]. Then, there is a wide range of **scanning force** microscopies, such as Magnetic Force Microscopies [6], which senses the stray field emanating from the specimen, or Nitrogen Vacancy (NV) center scanning probe microscopy [7], which has the potential to reach down into an atomic scale spatial resolution with nearly single spin sensitivity.

The interaction of **electrons** with the magnetic induction via the Lorentz force is utilized in transmission electron microscopies and with the availability of aberration corrected electron systems, they are pushing also towards highest spatial resolution in magnetic imaging [8]. Several approaches to implement fast pulsing into the Transmission Electron Microscope (TEM) column has opened avenues towards studies of ultrafast magnetization dynamics, although the intensity of electron sources seems to be a limiting factor [9]. Many other electron-based techniques such as Scanning Electron Microscopy with Polarization Analysis (SEMPA) [10] or Spin Polarized Low Energy Electron Microscopy (SPELEM) are also available for magnetic characterization specifically in the context of surface dominated magnetization processes [11].

Although **X-rays** have been discovered by W.C. Roentgen more than 120 years ago, and their short wavelength was immediately realized to resolve crystal structures, the fact that the refractive index is close to one has prevented them to be used in high resolution imaging techniques due to the lack of available X-ray optics. The development of nanostructuring techniques, e.g. nanolithography which was first used for semiconductor technologies opened the door to develop Fresnel zone plates with structures in the sub-100 nm regime, which allowed finally to focus X-rays and develop the first X-ray microscope (XRM) in the mid-1980 s [12]. Coincidentally, synchrotron radiation sources harnessing the radiated energy from high-energy physics circular accelerator became available at the same time and fostered the development of two major X-ray microscopy classes using those FZPs, i.e. full-field transmission X-ray microscopy (TXM) and scanning transmission X-ray microscopy. The water window around 2.4 nm photon wavelength, was the first major application with soft XRM as a powerful tool to study biological systems in their natural environment, including detailed tomographic reconstructions of whole cells due to the high penetration power of soft X-rays at this energy [13–15].

Initially, the sources for those X-rays were bending magnets at the storage rings, but with the advent of 3rd generation SR facilities the evolution of undulator devices at dedicated synchrotron sources provided much more brightness which benefitted largely most of the XRM technologies and with tunable polarization properties [16–18].

Polarized X-rays have been proven to be the key ingredient for studying magnetic materials. In analogy to the magneto-optical effects,

magnetic X-ray dichroism effects notably in the soft X-ray regime were discovered [19] that provide unique insight into nanomagnetic phenomena [20]. Subsequently, a plethora of magnetic X-ray spectro-microscopy techniques have been developed so far that have been applied to numerous systems, including magnetic thin films and patterned nanostructures [21]. There are circular and linear X-ray magnetic dichroism effects with the largest effects occurring in the soft X-ray regime, i.e., at L X-ray absorption edges of 3D transition metals, such as Fe, Co, Ni, as well as the corresponding M–edges in rare earth systems [22]. Those are the most prominent magnetic elements, which are also used in nearly all magnetic applications due to their outstanding magnetic properties, such as large magnetic moments in the 3d metals or the large orbital angular momentum in the rare earths. For example, Nd₂Fe₁₄B and Sm₂Co₅ provide still the strongest permanent magnets with the largest energy products BH_{max} [23], permalloy (Ni₂₀Fe₈₀) is a common soft magnetic material [24], and FeCr multilayers led to the discovery of giant magneto resistance (GMR) in 1988 [25,26], which completely transformed the magnetic storage technology and was awarded with the Nobel Prize in Physics in 2007. The proximity of 5d elements with their very large spin-orbit coupling to 3d elements in thin films has led to the discovery of novel topological spin textures [27], such as skyrmions [28] or Hopfions [29] at room temperature, which is among the latest research focus in the field of mesoscopic magnetic materials [30,31].

In the following, this article will focus exclusively on the use of polarized X-rays to characterize magnetic materials. It will briefly review some of the experimental details showing the breadth and complementary information that can be obtained and provide some examples from recent research activities to investigate the static and dynamic properties of novel topological spin textures, specifically magnetic vortices, skyrmions and Hopfions.

2. Experimental details

2.1. XMCD and XMLD spectroscopies

The interaction of polarized X-rays with magnetic materials can be divided into two major dichroism effects, that are being used to study various magnetic phenomena. X-ray magnetic circular dichroism (XMCD) is sensitive to the local magnetization $\langle \mathbf{M} \rangle$ and is being primarily used to study ferro- and ferrimagnetic materials, whereas X-ray magnetic linear dichroism (XMLD) is sensitive to $\langle \mathbf{M}^2 \rangle$ and has found wide applications to study antiferromagnetic materials [20].

Both occur in the vicinity of element-specific X-ray absorption edges, and therefore provide the inherent elemental-sensitivity to any technique that utilizes those effects.

XMCD measures the difference in X-ray absorption for parallel and antiparallel alignment of the magnetization relative to the propagation direction of the circularly polarized X-rays. It can be determined by either keeping the magnetization constant and vary the polarization or by changing the magnetization direction for fixed polarization. Since the magnetization in magnetic microstructures, i.e., in the magnetic domains are by definition pointing into different directions, a spatially resolved measurement of XMCD allows to use XMCD as magnetic contrast mechanism, which is the basic principle of magnetic X-ray microscopies in ferro- and ferrimagnetic materials. Large XMCD effects up to tens of percent occur at the spin-orbit coupled L edges of d transition metals (TM), and the M edges of 4f (rare earth (RE)) materials, all of them are basic components for most magnetic materials. For the 3d TMs and the RE elements those edges are in the soft X-ray energy range, i.e., between about 600–1400 eV, which are abundantly available at dedicated synchrotron radiation facilities worldwide. The hard X-ray regime covers the L edges of 5d TMs, which show reasonable XMCD effects in the few percent regime. There are also the K edges of TMs, notably the Fe K edge at 7.1 keV, where XMCD effects were first discovered in polarized X-ray absorption spectroscopy measurements

[32], however due to the lack of spin-orbit coupling at the K edge, which is a s-to-p electronic transition, the XMCD effects are minute and only rarely used. The much larger penetration power at harder X-rays, which is a clear advantage for bulk systems that would be also studied with polarized neutrons, can also be a curse particularly when the interesting samples are thin films with thicknesses in the few tens of nm regime.

With the discovery of the large XMCD effects in 3d TMs and the concurrent development of magneto-optical sum rules [33,34], that allow to quantitatively measure local spin and orbital magnetic moments, XMCD spectroscopy became an inevitable tool in studying fundamental phenomena in mesoscopic materials [21].

The second major X-ray dichroism effect is XMLD, which is primarily used to study antiferromagnetic materials [35,36]. Those effects are somewhat smaller than XMCD. Whereas the XMCD effects in single component 3d TMs are rather broad across the absorption lines, and exhibit a characteristic sign reversal from the L₃ to the L₂ edge due to the reversal of spin-orbit coupling their XMLD counterparts occur within a single L₃ or L₂ line and therefore require higher spectral resolution in the X-ray spectroscopy. For most X-ray spectroscopy beamlines, which include a high-performance monochromator device, this is well within the spectral resolving power and has led to highly accurate XMCD and XMLD spectroscopy measurements today.

Soon after XMCD and XMLD spectroscopies were established and could also be quantitatively analyzed, first experiments were performed to combine those dichroism effect with spatial resolution, i.e., the development of magnetic X-ray microscopies was launched using now XMCD and XMLD as contrast mechanism to create X-ray images of the magnetic domain patterns with much higher spatial resolution than with MO techniques [37,38]. Today, there is a variety of X-ray microscopy available which can be divided into two major categories, real space imaging devices, which create directly an image of the magnetic structures, and reciprocal space microscopies, who use scattering or X-ray diffraction patterns, where the information of the underlying microstructures is obtained either through a detailed interpretation of the scattering features or retrieved as real images through powerful computational algorithms, such as in ptychography. The real space techniques use either electron or X-ray optical elements, whereas the reciprocal technique will benefit largely from the upcoming increases in X-ray coherence at next generation light sources and the availability of high performance AI/ML driven data analysis tools.

2.2. X-ray photoelectron emission microscopy (X-PEEM)

The first magnetic images were recorded with X-PEEM [37]. There, circularly polarized X-rays, which are these days mostly emitted from polarized helical undulators (EPU) are monochromatized, e.g., by a plane grating monochromator (PGM) and illuminate the sample at an oblique angle. Since the XMCD effect is proportional to the projection of the X-ray beam onto the photon propagation direction, X-PEEM has a large sensitivity to the in-plane component of magnetization in the sample. Secondary electrons are created during the X-ray absorption process and can escape the sample's surface from within a limited depth of a few nm only, which makes X-PEEM highly surface sensitive. A large potential difference between the electron column and the sample pulls those electrons into the electron column of the PEEM, where they get transferred to a 2D detector, generally a CCD, where the location on the detector allows to determine the sample location, where it originated, i.e., the CCD signal is an image of the magnetization on the sample. Spatial resolutions, which have recently been improved through the implementation of aberration corrections into the PEEM system [39], can reach down into the few tens of nm regime [40], with about 30–50 nm being a standard resolution in magnetic imaging. The fact that X-PEEM detects the electrons limits severely the recording of magnetic structures within varying magnetic fields. To study the spin dynamics of magnetic nanostructures with X-PEEM utilizing the sub-100 ps time structure of SR sources, stroboscopic pump-probe schemes have been

used, where the pump-pulse was realized via an optically driven Auston switch to create short magnetic field pulses to the magnetic nanostructure [41]. The recent interest in 3d magnetic nanostructures, and curvilinear magnetism was approached by X-PEEM by analyzing the electrons that are created on the substrate after the X-rays have transmitted a specimen. 2d projections of the magnetic domain patterns can be combined into a 3d tomographic representation by recording those projection as function of a rotation angle of the sample [42,43].

Interfacial sensitivity has been probed with X-PEEM in a standing wave geometry [44], where the emitted PES signal was analyzed as a function of the Bragg angle, which moved a standing wave, that was created by an underlying multilayer structure, through the interfaces.

2.3. X-ray microscopies using X-ray diffractive optics

Complementary to X-PEEM there are two concepts for magnetic X-ray microscopy using X-ray diffractive optics, the full-field transmission X-ray microscope (TXM) [45,46] and the scanning transmission X-ray microscope (STXM) [47,48]. Fresnel zone plates, which are circular gratings are either used as imaging optics creating a high spatial resolution image in TXM or as focusing optics to create a small illumination spot in STXM, which is then raster scanned to create a real space image. Both bending magnets and undulators provide X-rays to TXMs and STXMs at various facilities worldwide, although most TXMs use the lower coherence light from a bending magnet, whereas STXMs benefit from the larger coherence at undulators, and in the future from the coherence in advanced storage rings.

Although in STXM a variety of detection mechanisms can be applied, MTXM and STXM are primarily photon-in/photon-out techniques, which means that external parameters, such as a magnetic field do not disturb the signal and magnetic images can be recorded throughout full hysteresis cycles to understand the relationship between magnetic microstructures and macroscopic magnetic quantities. The spatial resolution is primarily determined by the quality of the X-ray optics. Although values down the sub-10 nm regime have been reported [49,50], the standard resolution is about 20–30 nm, which is slightly better than with X-PEEM. MTXM and STXM do not require UHV conditions as X-PEEM, which has advantages, e.g., to excite the magnetic structure with field or current pulses in time-resolved stroboscopic pump-probe experiments [51,52]. The single point detection scheme in a STXM is advantageous specifically for time resolved magnetization studies, as single photons can be counted [53]. Although a few studies with a gated CCD have been reported with time-resolved MTXM [54], so far, time resolved MTXM studies used a two-bunch mode of the storage ring [55]. However, since those studies have a very low duty cycle and cannot be efficiently used in the typical multi-user environment at a large user facility, those special operational modes have started to phase out at various SR facilities.

The parallel data acquisition scheme is advantageous for multidimensional imaging, e.g., tomography, which has become an area of growing interest recently for magnetic systems [56–63]. An angular series of 2d projection images is recorded to apply tomographic reconstruction algorithms that allow to retrieve the 3d arrangement of spins inside the sample [64]. This approach has been routinely applied to cell imaging with TXM [65]. Due to the vector character of magnetization, and unless certain conditions can be assumed, a single rotation axis is not sufficient to derive the full 3d character of the magnetic moments.

To image interfaces, which can be seen as a subtopic for 3d imaging techniques, reflection geometries are considered [66–68], but so far, there is no dedicated TXM system that would allow such experiments.

2.4. Microscopies using X-ray scattering

The ongoing developments towards increasing the coherence at next generation light sources is to a large extend also motivated by the fact that diffraction-based imaging methods will tremendously benefit from that coherence [69–72]. Most importantly is the fact, that in the real

space imaging techniques mentioned so far, only the intensity can be retrieved, but apart from including special X-ray optical elements, the phase is generally lost. However, phase contrast has not only a major advantage for low intensity contrast specimens [73,74], but the phase itself is a highly sensitive experimental parameter, which has the prospect to be characterized with unprecedented precision physical phenomena, allowing measuring minute spin currents through interfaces, etc.

Among those diffraction-based imaging methods are ptychography techniques [75–81], which are based on the concept to use a STXM in combination with a CCD detector to record for every scanning step a full diffraction pattern of the sample. This oversampling and large data sets can be used to retrieve with powerful algorithms and computing power both amplitude and phase of the signal. In addition, they are expected to increase the spatial resolution down to the diffraction limit of X-rays, which would be in the few nm regime for soft X-rays and in the atomic regime for hard X-rays [76].

So far, promising pioneering experiments have been performed showing the potential to increase spatial resolution [76,77]. Very recently, first experiments have been done with hard X-ray ptychography to resolve the complex spin textures in bulk magnetic materials in the vicinity of Bloch points [61], which are magnetic singularities with far reaching impact to fundamental problems in magnetism. Another variant in this category is X-ray laminography, which has even presented its feasibility for adding time resolution to those techniques [60].

3. Results

Although the static microscopic spin texture in mesoscopic magnetic materials is the result of minimizing the Gibbs Free Energy, i.e., resulting from the competition of various energies such as exchange (Heisenberg or Dzyaloshinskii–Moriya) interactions, magneto-crystalline anisotropies, dipolar or Zeeman interaction, it has been recently recognized that topology itself has a deep impact to magnetism, and as such to the formation of those spin textures [82–86].

Topology is a field of mathematics which studies the properties of objects which are preserved under smooth deformations in a continuum limit [87–92]. Since magnetic materials cannot exactly be described as a continuum, as the magnetic moments are localized at atomic sites, which is particularly true for the description of magnetic phenomena within a micromagnetic model, the topology of a spin texture can change. However, topology also provides a certain level of protection, which implies that a certain spin texture cannot be unwound without creating singularities, such as a Bloch point [93]. This protection could be technologically advantageous, if those topological spin textures were used in future applications [30,94–96]. Finally, topology also has a profound impact on the dynamics of those novel spin textures [97–99], and therefore studying the static and dynamics of topological spin textures is an area of great current interest.

3.1. Magnetic vortex dynamics

As a first example, we will discuss briefly a time-resolved MTXM study to investigate the current induced dynamics of a vortex core in a permalloy nanodisk.

The magnetic ground state in a lithographically defined circular permalloy disk with a diameter in the micrometer range and thicknesses in the tens of nm regime, is the vortex structure (VS) [100–102]. For larger heights and smaller radius, a perpendicular single domain state replaces the vortex state. The VS is composed of a circulating in-plane texture, which can be pointing clock-wise (CW) or counter-clock-wise (CCW) (circularity), following the shape of the disk to minimize shape anisotropy. However, towards the center of the disk, i.e., [103] for circles with decreasing radius, the increase in exchange energy from neighboring spins pointing more and more antiparallel to each other is released by an out-of-plane components, that can point up or down

(polarity) which forms the so-called vortex core in the center or a disk. With both circularity and polarity having two independent values for up/down and CW/CCW, the vortex state has four degenerate ground states [104,105]. Those magnetic vortices were first experimentally imaged with MFM in a seminal paper by Shinjo *et al.* [100] and have seen an enormous research effort soon after that [41,106–126]. The core dynamics can be excited by magnetic and current pulses, and Fig. 1 shows the results of a time-resolved MTXM study to investigate the current-induced vortex dynamics [108]. Fig. 1a shows the schematic pump-probe setup, where the electronic pump pulse was synchronized to the 3 MHz RF of the storage ring, which is the frequency of the probing X-ray pulse. Varying the delay between the pump and the probe pulse up to about 10 ns, a sequence of images of the VC was obtained (Fig. 1b) showing the gyration motion of the VC inside the disk. The high spatial resolution of MTXM allowed to measure the gyration radius as a function of the excitation frequency (Fig. 1c). Applying the Thiele equation enabled a quantitative determination of the polarization of the excitation current, which was in excellent agreement with expectations [108].

3.2. Magnetic skyrmion dynamics

The topic of topology in magnetic systems started to attract significant attention with the first observation of magnetic skyrmions in B20 compounds such as MnSi, FeCoSi and FeGe, where the non-centrosymmetric crystal structure provided the requisite inversion symmetry breaking that gave rise to a bulk DMI [127,128]. Despite the scientific excitement of this pioneering work and the perspective to utilize those skyrmions as small, fast and resilient building blocks in future spintronics [95], those skyrmions were unfortunately only stable at low temperatures and in external magnetic fields, which made them less appealing for potential applications.

However, it was soon realized that DMI can also emerge at interfaces due to the broken mirror symmetry, which launched a race in the community towards identifying magnetic multilayer systems where stable magnetic skyrmions would exist at room temperature. In 2016, several papers were able to report the successful creation and observation of magnetic skyrmions at room temperature [129–132].

Different types of magnetic skyrmions are characterized by the way that their magnetization structure changes from the core to the outside. Generally, for Bloch-type skyrmions the magnetization rotates perpendicular to the radial direction, whereas for Néel-type skyrmions it rotates along this direction. The topology of skyrmions is represented by the skyrmion number topological invariant. The skyrmion number is obtained by the integration of a two dimensional topological charge, i.e., the winding number, which counts how many times the spin texture wraps the 2D surface of a 3D sphere [133]. It is defined by $N_{sk} = \frac{1}{4\pi} \iint d^2r m \cdot (\frac{\partial m}{\partial x} \times \frac{\partial m}{\partial y})$ with m being the unit vector of the magnetization. Néel- or Bloch-type skyrmions have $N_{sk} = -1$ for the core magnetization pointing into the negative z-direction. As another reference, a meron (or a magnetic vortex) has $N_{sk} = -0.5$. To fully describe the magnetization texture of skyrmions, there are two other characteristic numbers, the vorticity, which describes the in-plane spin texture, and the helicity, which takes the role of a phase in describing the vorticity [133].

Fig. 2 shows the result of a study of magnetic skyrmions and their current driven motion in thin transition metal ferromagnets at room temperature [130]. The systems chosen were {Pt(3 nm)/Co(0.9 nm)/Ta(4 nm)}₁₅ and {Pt(4.5 nm)/CoFeB(0.7 nm)/MgO(1.4 nm)}₁₅ multilayer stacks which were fabricated by established DC magnetron sputtering, and exhibited a pronounced perpendicular magnetic anisotropy. To image the static skyrmion spin texture and specifically also their current-driven dynamics using both full-field MTXM and time-resolved STXM those multilayers were deposited onto X-ray transparent 100 nm thin Si₃N₄ membranes.

Fig. 2a shows a sketch of the sample geometry. A current pulse was launched from the yellow pad to create individual skyrmions and to

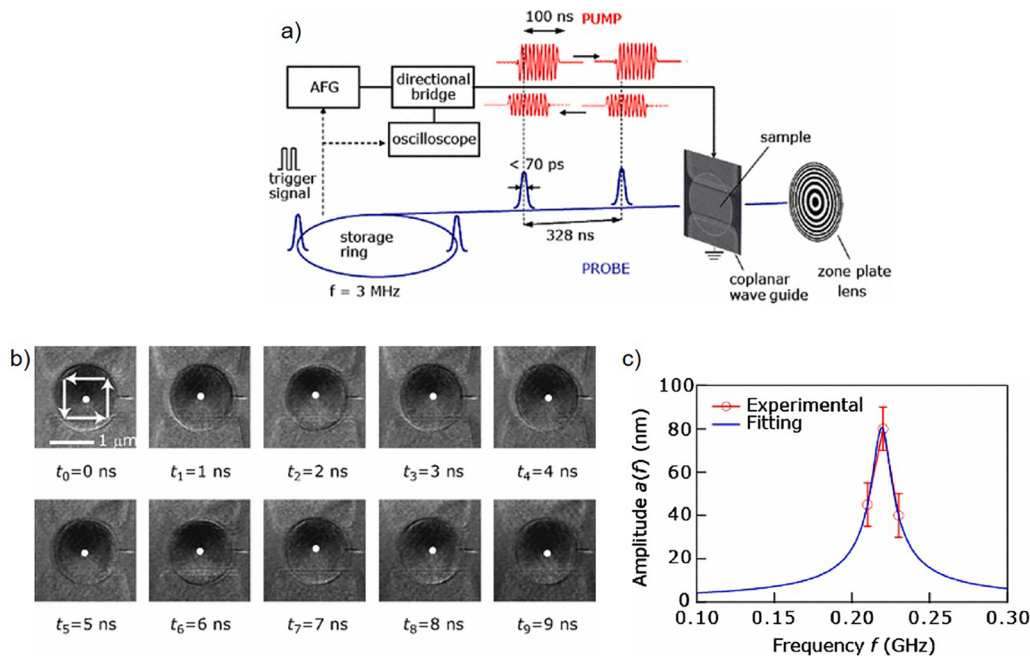


Fig. 1. a) Schematic experimental setup for stroboscopic pump–probe time resolved magnetic transmission soft X-ray microscopy in 2-bunch mode operation of the storage ring. b) Sequence of MTXM images for delay times between pump and probe between 0 ns and 9 ns showing the gyration motion of the vortex core (white point). The arrows indicate the orientation of the in-plane magnetization following the shape of the disk. c) Amplitude of gyration motion as function of the excitation frequency. The fitting line (blue) is derived from the Thiele equation, the experimental data points match well the model. Reprinted figure with permission from S. Kasai et al Phys Rev Lett 01 237,203 (2008) Copyright (2008) by the American Physical Society.

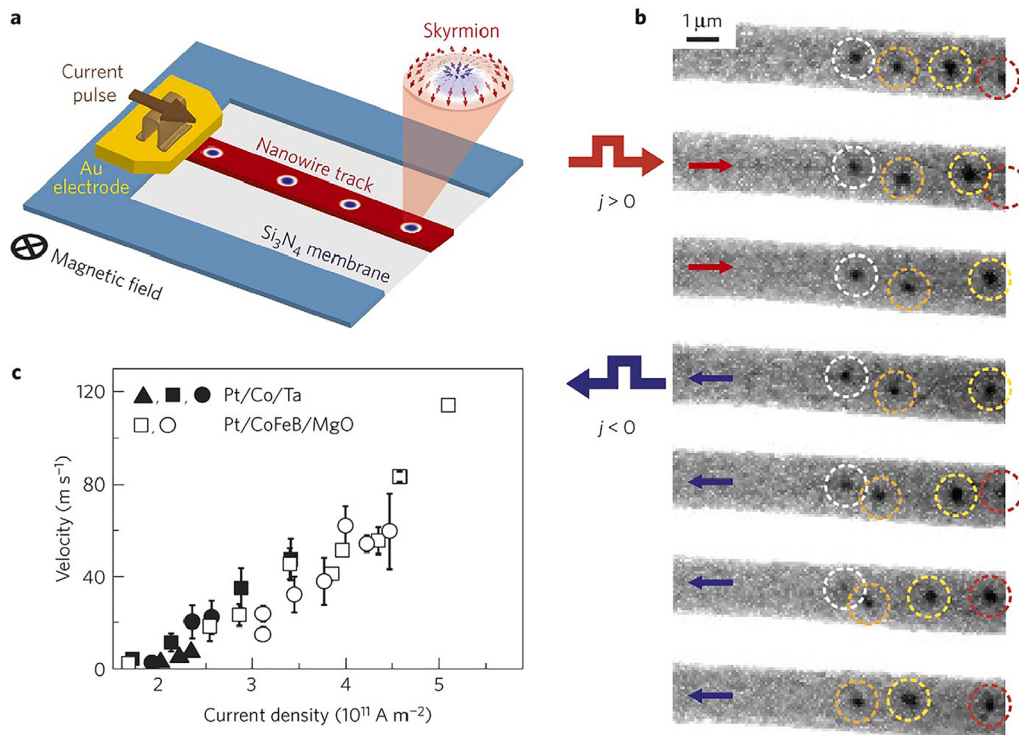


Fig. 2. a) Schematic experimental setup for MTXM measurement of individual skyrmions injected into and moving along a racetrack. The nanowire track is deposited onto an X-ray transparent Si_3N_4 membrane, external fields are applied perpendicular to the membrane surface, and an Au electrode is used to launch current pulse into the track. b) Sequence of magnetic X-ray microscopy images showing a train of individual skyrmion as they are pushed by individual current pulses. c) Velocity of skyrmions as a function of current density. Reprinted with permission by Springer Nature from S. Woo et al Nature Materials 15 501 (2016).

push them along the nanowire, which resembles a so-called racetrack geometry, which was introduced by Parkin et al to move domain walls as units of information. An analysis of the measured domain width in those multilayers, which were imaged by high resolution MTXM allowed to derive the DMI strength and an examination of bubble domain expansion has proven DMI-stabilized Néel domain walls with left-handed chirality, as expected because of the strong interfacial DMI in those systems

Measuring the velocity as a function of current density, skyrmion speeds up to 100 m/s were found, which seem to be well suited for

potential ultrafast devices (Fig. 2b). Finally, first results of observing the interesting spin dynamics is shown in Fig. 2c, which shows the ability to push the skyrmions along the racetrack by consecutive individual short electronic pulses. However, it was also noticed, that the imperfections of the multilayers, e.g., defect could trap individual skyrmions, which would then annihilate with other skyrmions in this track [130].

3.3. Ultrafast spin fluctuations on the nanoscale

Whereas the previous study aimed at investigating the deterministic

dynamics of magnetic skyrmions, which is required to reliably operate skyrmion based devices, the non-deterministic fluctuations of spin textures specifically on the nanoscale have been an interesting topic for a long time [134]. To explore those length and time scales, X-ray Free Electron Laser facilities are providing the requisite probe, as they can deliver ultrashort and high intense X-ray pulses with appropriate wavelengths, photon energies and polarization [72]. Among the many new techniques to study materials properties in an unprecedented fashion, we want to mention the X-ray photo correlation spectroscopy [135,136] and in particular the recently developed two pulse mode, which enables to study spontaneous fluctuations on nanosecond time scales in nanoscale materials [137]. Those spontaneous fluctuations are known to impact materials properties, such as transport, or viscosity [138]. Fig. 3 shows the results from a study, where two-pulse XPCS was used to investigate the ultrafast spin fluctuations in a Fe/Gd multilayer systems [137]. Using resonant soft X-ray scattering and Lorentz TEM, it was shown that this system exhibits at room temperature upon applying an external magnetic field a phase transition from a stripe phase to a skyrmion lattice phase. The experiments at LCLS revealed that the spin fluctuations near the stripe-to-Skyrmion phase boundary exhibit drastic changes. Fig. 3b and c show the magnetic contrast of the system as a function of the delay time between the two subsequent pulses. There are drastic differences in the decay times for the two phases, which reflects significant modifications of characteristic correlation times for those two phases.

3.4. Resolving the spin structure in magnetic Hopfions

Although the description of magnetic skyrmions assumes a 2D magnetization texture, in real systems, e.g., thin films, their textures extend into the third dimension [56,139]. Therefore, a generalization of the concept of magnetic skyrmions into the third dimension leads to more complex topological solitons with new topological invariants, including rings, knots and links [87,91,140,141]. Examples that have attracted recent scientific interests include skyrmion tubes [142,143], chiral bobbers [144–146], torons [147,148], vortex rings [149] and Hopf solitons, or Hopfions [29,150–154].

The latter can be classified by a topological invariant, the Hopf number (Q_H), which in real space can be expressed as $Q_H = -\int \mathbf{B} \cdot d\mathbf{A}^3$ with \mathbf{B} being the emergent magnetic field from the spin texture and \mathbf{A} the

magnetic vector potential [155]. The Hopf number distinguishes the topology in different Hopfions and can be geometrically interpreted as the linking number of any two closed-loop regions in 3D real space that contains spins pointing in the same direction, so called isosurfaces of magnetization [89,154]. A Hopfion can also be considered as a twisted, closed loop of Skyrmion string, where the Hopf number is the number of twists.

Hopfions with micrometer sizes have been experimentally observed e.g., in fluid chiral ferromagnets and liquid crystals [89,140]. Hopfions in solid chiral magnets were elusive until recently the combination of various advanced magnetic X-ray spectro-microscopies allowed the first experimental verification of such magnetic Hopfions [29].

To that end, Target Skyrmions, which are extended skyrmion textures, where the magnetization rotates multiple times were predicted from theory as pre-cursors for magnetic Hopfion [2,154,156,157]. Using MTXM TSKs were observed in magnetic multilayers with a strong DMI and PMA. Permalloy nanodisks grown on top of the multilayers stabilized the TSKs in the multi-layer through structural imprinting mediated by the long-range dipole interaction [158]. To stimulate the formation of a magnetic Hopfion, the multilayer known to host TSKs was patterned into disks. A changing profile of the PMA across the thickness – high on the top and bottom, low in the middle – allowed for the stabilization of Hopfions rather than TSKs.

Fig. 4 shows the results of a recent X-ray spectro-microscopy study to confirm the stabilization of magnetic Hopfions in such patterned multilayers [29]. Fig. 4a and b shows the schematics of the spin texture of a TSK and a Hopfion. Whereas the TSK does not show variations across the disk thickness, the design of the PMA profile forces the spins to form a twisted skyrmion tube inside the disk. The striking difference of the magnetization structures particularly at the top surface between the TSK and the Hopfion lends itself to using the surface sensitive X-PEEM and compare it with bulk sensitive MTXM to get access to both regions in the magnetic nanostructure.

Fig. 4c and d show simulated experimental profile for a Hopfion, when imaged with those complementary techniques. Experimental data are presented in Fig. 4e and f, where Fig. 4f shows X-PEEM results recorded at varying inclination angle, so that a full 3D reconstruction of the near-surface magnetization texture could be obtained and compared to the expected simulated data in Fig. 4a. Fig. 4g and h clearly prove the agreement between expected simulation and experiment, which lead to

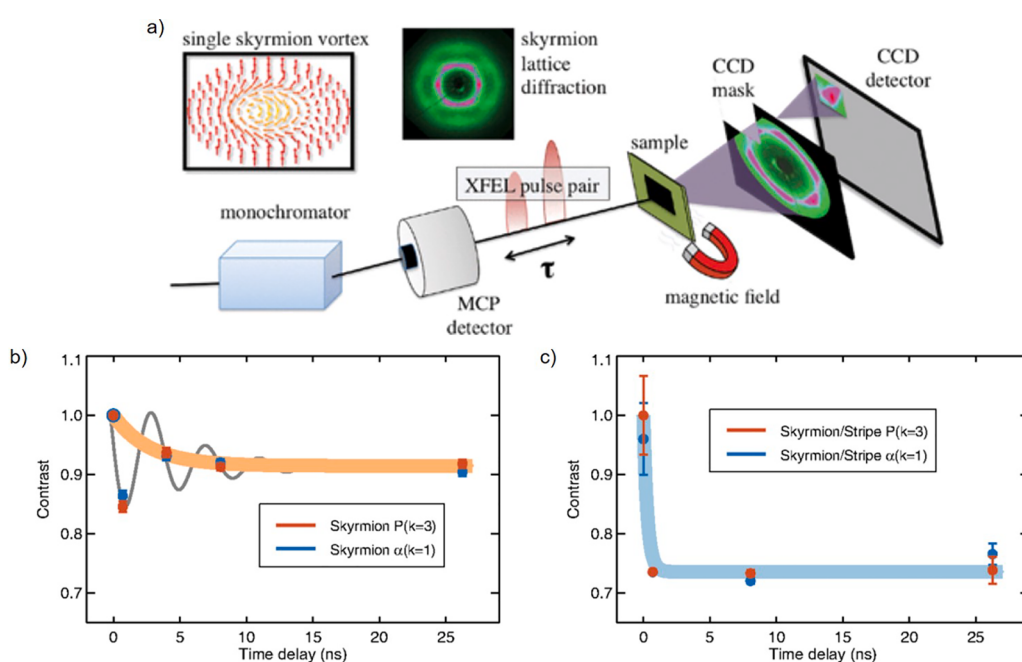


Fig. 3. a) Schematic experimental setup for the 2-pulse XPCS at LCLS in Stanford. The insets show the spin texture of a single skyrmion vortex and the hexagonal X-ray diffraction pattern reminiscent of a skyrmion lattice. b), c) Contrast as a function of delay time between the two consecutive pulses for the skyrmion lattice phase (b) and the skyrmion stripe phase (c) showing a remarkable change in the decay times of the contrast. Reprinted from M. Seaberg et al, Phys Rev Lett 119 067,403 (2017).

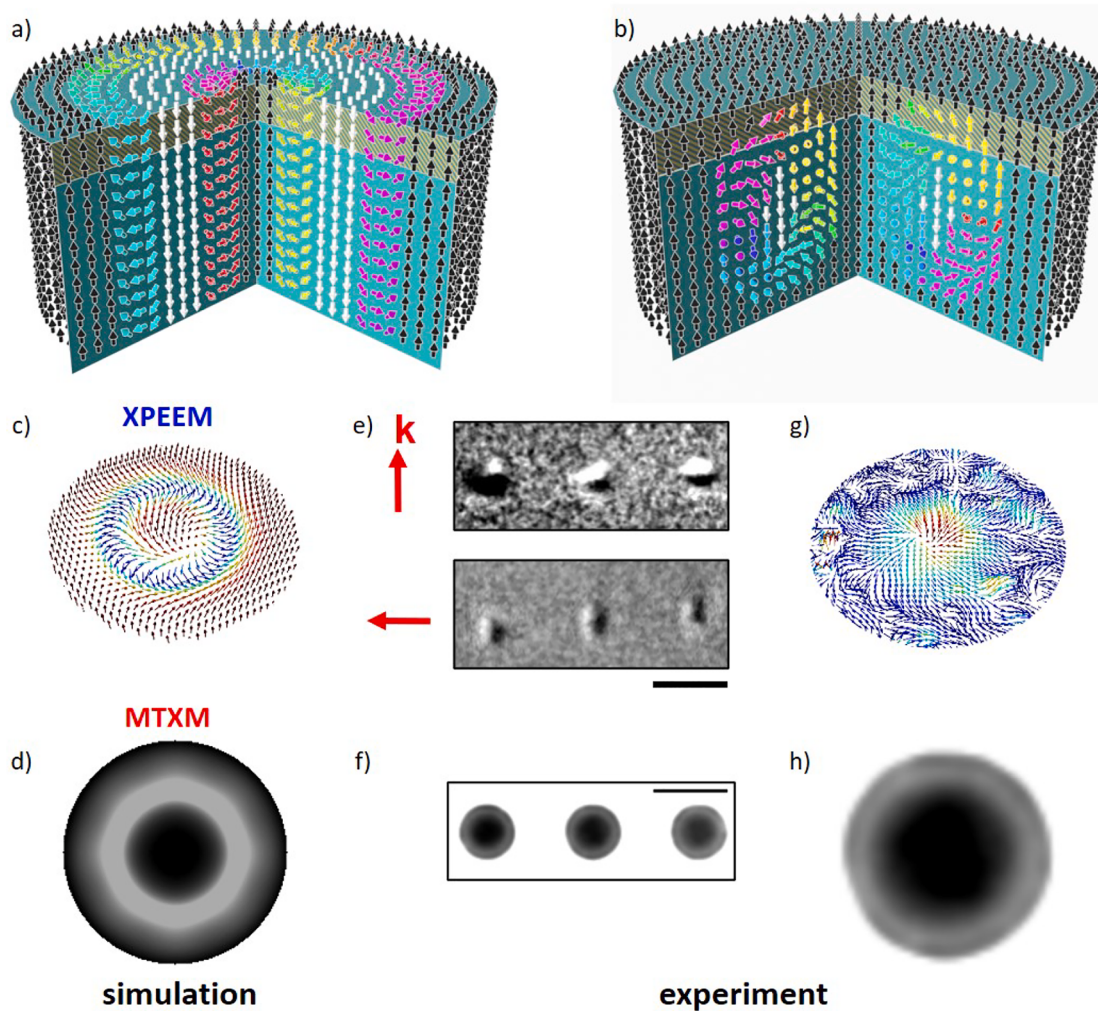


Fig. 4. Schematic spin texture in a nanodisk for a) the Target Skyrmion and b) the Hopfion, showing the stark differences throughout the thickness of the disk. c, d) Simulations of the expected X-PEEM and MTXM contrast for the Hopfion structure. e) X-PEEM data for two orthogonal orientation relative to the incoming photon beam, which are used to obtain a 3D reconstruction of the near-surface magnetization. f) Representative experimental MTXM data. g), h) Experimental data for X-PEEM and MTXM showing good agreement with the expectations. Reprinted and adapted from N. Kent et al Nature Comm 12 1562 (2020).

the conclusion that the specifically designed magnetic system following theoretical predictions enabled the stabilization of the magnetic Hopfion spin textures. [29]

Magnetic Hopfions are predicted to have interesting and characteristic dynamics [151,152]. Most notably is the feature, that unlike magnetic skyrmions which experience a Magnus-force-like deflection in a racetrack geometry, the vanishing gyrovector in magnetic Hopfions can have significant advantages in Hopfion-based applications.

So far, detailed simulation studies of Hopfion dynamics have been performed, including current-induced and field-driven studies up to high frequencies. The former show interesting and complex tumbling and breathing dynamics in three dimensions[152], whereas the latter include a transition from a Hopfion to a toron structure with pronounced resonant frequencies, that could also open a path towards identifying Hopfions from other topological 3D mesoscopic spin textures with time resolved advanced magnetic X-ray spectro-microscopies.

4. Future opportunities

Mesoscopic magnetic materials are among the most promising candidates for low-power, highly efficient, multifunctional devices which will be the backbone of the future information technology. Of paramount importance will be advanced characterization techniques to validate their performance across multiple length and time scales to

determine properties that can be exploited in future spintronic applications. Magnetic X-ray spectro-microscopies have the potential to cover in a unique way both spatial, temporal and multidimensional requirements in concert with inherent elemental and quantitative sensitivities. Numerous X-ray techniques have been developed, many of them were transformed to magnetic characterization tools by using the unique features of polarization in the X-rays. A similar transformation can be expected from harnessing the inherent full coherence, both spatially (transversal) as well as temporal (longitudinal) coherence. One of the parameters of X-rays that will be accessible with coherent X-rays is the phase of the X-rays itself, which will allow unprecedented sensitivities, e.g., to detect minute spin currents, or characterize variations on the spin texture at length scales, which touch the ultimate limits of current physics.

Electron microscopies, which are inherently much more sensitive to external parameters, such as magnetic fields or electric currents, than their X-ray counterparts, are not only leading in their capability to resolve sub-atomic structures, but they are also seeing analogous developments, e.g., with regard to electron beams with large angular orbital momentum [159], or efforts to introduce ultrafast temporal resolution [160], such as Ultrafast Electron Diffraction [161] or laser-triggered electron sources [162].

Therefore, it can be expected that the future research on mesoscopic magnetic materials will take more and more advantage of the

complementarity between electron and X-ray based spectro-microscopies.

Declaration of Competing Interest

The authors declare that they have no known competing financial interests or personal relationships that could have appeared to influence the work reported in this paper.

Acknowledgements

This work was supported by the U.S. Department of Energy, Office of Science, Office of Basic Energy Sciences, Materials Sciences and Engineering Division, under Contract No. DE-AC02-05-CH11231 within the Non-Equilibrium Magnetism program (MSMAG).

References

- [1] S.D. Bader, S.S.P. Parkin, Annu. Rev. Condens. Matter Phys. 1 (1) (2010) 71–88.
- [2] A. Hubert, R. Schäfer, *Magnetic Domains: The Analysis of Magnetic Microstructures*, Springer, 1998.
- [3] I. Dzyaloshinsky, J. Phys. Chem. Solids 4 (4) (1958) 241–255.
- [4] J. McCord, J. Phys. D Appl. Phys. 48 (33) (2015), 333001.
- [5] R. Wiesendanger, Rev. Mod. Phys. 81 (4) (2009) 1495–1550.
- [6] O. Kazakova, R. Puttock, C. Barton, H. Corte-León, M. Jaafar, V. Neu, A. Asenjo, J. Appl. Phys. 125 (6) (2019), 060901.
- [7] J.P. Tetienne, et al., Science 344 (2014) 1366.
- [8] C. Phatak, A.K. Petford-Long, M. De Graef, Curr. Opin. Solid State Mater. Sci. 20 (2) (2016) 107–114.
- [9] S. McVittie, D. McGrouther, S. McPadzean, D.A. MacLaren, K.J. O’Shea, M. J. Benitez, Ultramicroscopy 152 (2015) 57–62.
- [10] F. Kloodt-Tweten, S. Kuhrau, P. Staek, D.R. Cavicchia, F. Lofink, H.P. Oepen, R. Frömler, Phys Rev B 97 (2) (2018), 024426.
- [11] G. Chen, S.P. Kang, C. Ophus, A.T. N’Diaye, H.Y. Kwon, R.T. Qiu, C. Won, K. Liu, Y. Wu, A.K. Schmid, Nat. Commun. 8 (1) (2017) 15302.
- [12] D. Attwood, *Soft X-Rays and Extreme Ultraviolet Radiation: Principles and Applications*, Cambridge University Press, Cambridge, 1999.
- [13] D. Weiss, G. Siegmann, B. Niemann, P. Guttmann, D. Rudolph, G. Schmahl, Ultramicroscopy 84 (3–4) (2000) 185–197.
- [14] J. Guo, C.A. Larabell, Curr. Opin. Struct. Biol. 58 (2019) 324–332.
- [15] C.A. Larabell, M.A. Le Gros, Mol. Biol. Cell 15 (3) (2004) 957–962.
- [16] M.R. Weiss, R. Follath, K.J.S. Sawhney, F. Senf, J. Bahrdt, W. Frentrup, A. Gaupp, S. Sasaki, M. Scheer, H.C. Mertins, D. Abramsohn, F. Schäfers, W. Kuch, W. Mahler, Nuclear Instruments and Methods in Physics Research Section A: Accelerators, Spectrometers, Detectors and Associated Equipment 467–468 (2001) 449–452.
- [17] A.T. Young, E. Arenholz, S. Marks, R. Schlueter, C. Steier, H.A. Padmore, A. P. Hitchcock, D.G. Castner, Journal of Synchrotron Radiation 9 (4) (2002) 270–274.
- [18] G. Brown, K. Halbach, J. Harris, H. Winick, Nucl. Instrum. Methods Phys. Res. 208 (1) (1983) 65–77.
- [19] C.T. Chen, S. Modesti, Phys. Rev. 42 (1990) 7262.
- [20] J. Stoehr, H.C. Siegmann, *Magnetism: from Fundamentals to Nanoscale Dynamics*, 2006.
- [21] P. Fischer, H. Ohldag, Rep. Prog. Phys. 78 (2015) 9.
- [22] G.V.D. Laan, A.I. Figueroa, Coord. Chem. Rev. 277–78 (2014) 95.
- [23] J.M.D. Coey, Engineering 6 (2) (2020) 119–131.
- [24] H.D. Arnold, G.W. Elmen, Bell Syst. Tech. J. 2 (3) (1923) 101–111.
- [25] M.N. Baibich, J.M. Broto, A. Fert, F. Nguyen Van Dau, F. Petroff, P. Etienne, G. Creuzet, A. Friederich, J. Chazelas, Phys. Rev. Lett. 61 (21) (1988) 2472–2475.
- [26] G. Binasch, P. Grunberg, F. Saurenbach, W. Zinn, Phys. Rev. B 39 (7) (1989) 4828–4830.
- [27] A. Fert, F.N. Van Dau, C.R. Phys. (2019).
- [28] W. Jiang, G. Chen, K. Liu, J. Zang, S.G.E. te Velthuis, A. Hoffmann, Phys. Rep. 704 (2017) 1–49.
- [29] N. Kent, N. Reynolds, D. Raftrey, I.T.G. Campbell, S. Virasawmy, S. Dhuey, R. V. Chopdekar, A. Hierro-Rodriguez, A. Sorrentino, E. Pereiro, S. Ferrer, F. Hellman, P. Sutcliffe, P. Fischer, Nat. Commun. 12 (1) (2021) 1562.
- [30] C. Back, V. Cros, H. Ebert, K. Everschor-Sitte, A. Fert, M. Garst, T. Ma, S. Mankovsky, T.L. Monchesky, M. Mostovoy, N. Nagosa, S.S.P. Parkin, C. Pfleiderer, N. Reyren, A. Rosch, Y. Taguchi, Y. Tokura, K. von Bergmann, J. Zang, J. Phys. D Appl. Phys. 53 (36) (2020), 363001.
- [31] K. Everschor-Sitte, J. Masell, R.M. Reeve, M. Kläui, J. Appl. Phys. 124 (24) (2018), 240901.
- [32] G. Schütz, W. Wagner, W. Wilhelm, P. Kienle, R. Zeller, R. Frahm, G. Materlik, Phys. Rev. Lett. 58 (7) (1987) 737–740.
- [33] P. Carra, B.T. Thole, M. Altarelli, X. Wang, Phys. Rev. Lett. 70 (5) (1993) 694–697.
- [34] B.T. Thole, P. Carra, F. Sette, G. van der Laan, Phys. Rev. Lett. 68 (12) (1992) 1943–1946.
- [35] C. Luo, H. Ryll, C.H. Back, F. Radu, Sci. Rep. 9 (1) (2019) 18169.
- [36] G. van der Laan, N.D. Telling, A. Potenza, S.S. Dhesi, E. Arenholz, Phys Rev B 83 (6) (2011), 064409.
- [37] J. Stöhr, Y. Wu, B.D. Hermsmeier, M.G. Samant, G.R. Harp, S. Koranda, D. Dunham, B.P. Tonner, Science 259 (5095) (1993) 658.
- [38] P. Fischer, G. Schütz, G. Schmahl, P. Guttmann, D. Raasch, Zeitschrift für Physik B Condens. Matter. 101 (3) (1997) 313–316.
- [39] A.A. MacDowell, J. Feng, A. DeMello, A. Doran, R. Duarte, E. Forest, N. Kelez, M. A. Marcus, T. Miller, H.A. Padmore, S. Raoux, D. Robin, A. Scholl, R. Schlueter, P. Schmid, J. Stöhr, W. Wan, D.H. Wei, Y. Wu, AIP Conf. Proc. 879 (1) (2007) 1341–1344.
- [40] F. Kronast, N. Friedenberger, K. Ollefs, S. Gliga, L. Tati-Bismaths, R. Thies, A. Ney, R. Weber, C. Hassel, F.M. Römer, A.V. Trunova, C. Wirtz, R. Hertel, H.A. Dürr, M. Farle, Nano Lett. 11 (4) (2011) 1710–1715.
- [41] S.-B. Choe, Y. Acremann, A. Scholl, A. Bauer, A. Doran, J. Stöhr, H.A. Padmore, Science 304 (2004) 420.
- [42] J. Kimling, F. Kronast, S. Martens, T. Boehnert, M. Martens, J. Herrero-Albillos, L. Tati-Bismaths, U. Merkt, N. Nielsch, G. Meier, Phys. Rev. 84 (2011).
- [43] R. Streubel, F. Kronast, P. Fischer, D. Parkinson, O.G. Schmidt, D. Makarov, Nat. Commun. 6 (2015) 7612.
- [44] A.X. Gray, F. Kronast, C. Papp, S.-H. Yang, S. Cramm, I.P. Krug, F. Salmassi, E. M. Gullikson, D.L. Hilken, E.H. Anderson, P. Fischer, H.A. Dürr, C.M. Schneider, C.S. Fadley, Appl. Phys. Lett. 97 (6) (2010), 062503.
- [45] P. Fischer, T. Eimüller, G. Schütz, G. Denbeaux, A. Pearson, L. Johnson, D. Attwood, S. Tsunashima, M. Kumazawa, N. Takagi, M. Köhler, G. Bayreuther, Rev. Sci. Instrum. 72 (5) (2001) 2322–2324.
- [46] A. Sorrentino, J. Nicolas, R. Valcarcel, F.J. Chichon, M. Rosanes, J. Avila, A. Tkachuk, J. Irwin, S. Ferrer, E. Pereiro, J. Synchrotron Radiat. 22 (4) (2015) 1112–1117.
- [47] Y. Acremann, J. Strachan, V. Chembrolu, S. Andrews, T. Tyliaszak, J. Katine, M. Carey, B. Clemens, H. Siegmann, J. Stöhr, Phys. Rev. Lett. 96 (2006).
- [48] J. Raabe, G. Tsvetkov, U. Flechsig, M. Böge, A. Jaggi, B. Sarafimov, M.G. C. Vernooy, T. Huthwelker, H. Ade, D. Kilcoyne, T. Tyliaszak, R.H. Fink, C. Quitmann, Rev. Sci. Instrum. 79 (11) (2008), 113704.
- [49] W. Chao, P. Fischer, T. Tyliaszak, S. Rekawa, E. Anderson, P. Naulleau, Opt. Express 20 (2012) 9777.
- [50] J. Vila-Comamala, K. Jefimovs, J. Raabe, T. Pilvi, R.H. Fink, M. Senoner, A. Maassdorff, M. Ritala, C. David, Ultramicroscopy 109 (2009) 1360.
- [51] Y. Acremann, V. Chembrolu, J. Strachan, T. Tyliaszak, J. Stoehr, Rev. Sci. Instrum. 78 (2007).
- [52] A. Puzic, H. Stoll, P. Fischer, B.V. Waeyenberge, J. Raabe, G. Denbeaux, T. Haug, D. Weiss, G. Schütz, Phys. Scripta 1029 (2005).
- [53] S. Bonetti, R. Kukreja, Z. Chen, D. Spoddig, K. Ollefs, C. Schöppner, R. Meckenstock, A. Ney, J. Pinto, R. Houanche, J. Frisch, J. Stöhr, H.A. Dürr, H. Ohldag, Rev. Sci. Instrum. 86 (9) (2015), 093703.
- [54] P. Wessels, J. Ewald, M. Wieland, T. Nisius, G. Abatti, S. Baumbach, J. Overbuschmann, A. Vogel, A. Neumann, J. Viehhaus, H.P. Oepen, G. Meier, T. Wilhein, M. Drescher, J. Phys. Conf. Ser. 499 (2014), 012009.
- [55] H. Stoll, A. Puzic, B. van Waeyenberge, P. Fischer, J. Raabe, M. Buess, T. Haug, R. Höllinger, C. Back, D. Weiss, G. Denbeaux, Appl. Phys. Lett. 84 (17) (2004) 3328–3330.
- [56] A. Fernández-Pacheco, R. Streubel, O. Fruchart, R. Hertel, P. Fischer, R. P. Cowburn, Nat. Commun. 8 (2017) 15756.
- [57] P. Fischer, D. Sanz-Hernández, R. Streubel, A. Fernández-Pacheco, APL Mater. 8 (1) (2020), 010701.
- [58] R. Streubel, E.Y. Sybimal, P. Fischer, J. Appl. Phys. 129 (21) (2021), 210902.
- [59] C. Donnelly, S. Gliga, V. Scagnoli, M. Holler, J. Raabe, L.J. Heyderman, M. Guizar-Sicairos, New J. Phys. 20 (8) (2018), 083009.
- [60] C. Donnelly, S. Finizio, S. Gliga, M. Holler, A. Hrabec, M. Odstrčil, S. Mayr, V. Scagnoli, L.J. Heyderman, M. Guizar-Sicairos, J. Raabe, Nat. Nanotechnol. (2020).
- [61] C. Donnelly, M. Guizar-Sicairos, V. Scagnoli, S. Gliga, M. Holler, J. Raabe, L. J. Heyderman, Nature 547 (2017) 328.
- [62] K. Witte, A. Späth, S. Finizio, C. Donnelly, B. Watts, B. Sarafimov, M. Odstrčil, M. Guizar-Sicairos, M. Holler, R.H. Fink, J. Raabe, Nano Lett. 20 (2) (2020) 1305–1314.
- [63] D. Sanz-Hernández, A. Hierro-Rodriguez, C. Donnelly, J. Pablo-Navarro, A. Sorrentino, E. Pereiro, C. Magén, S. McVittie, J.M. de Teresa, S. Ferrer, P. Fischer, A. Fernández-Pacheco, ACS Nano 14 (7) (2020) 8084–8092.
- [64] R. Streubel, L. Han, F. Kronast, A.A. Ünal, O.G. Schmidt, D. Makarov, Nano Lett. 14 (7) (2014) 3981–3986.
- [65] D.Y. Parkinson, C. Knoechel, C. Yang, C.A. Larabell, M.A. Le Gros, J. Struct. Biol. 177 (2) (2012) 259–266.
- [66] S. Macke, E. Goering, J. Phys.: Condens. Matter 26 (36) (2014), 363201.
- [67] S. Brück, G. Schütz, E. Goering, X. Ji, K.M. Krishnan, Phys. Rev. Lett. 101 (12) (2008), 126402.
- [68] G. Denbeaux, P. Fischer, F. Salmassi, K. Dunn, J. Evertsen, Proc. 8th Int. Conf. X-ray Microscopy, 2006.
- [69] M. Eriksson, J.F. van der Veen, C. Quitmann, J. Synchrotron Radiat. 21 (5) (2014) 837–842.
- [70] B.W.J. McNeil, N.R. Thompson, Nat. Photonics 4 (12) (2010) 814–821.
- [71] N. Huang, H. Deng, B. Liu, D. Wang, Z. Zhao, Innov. 2 (2) (2021), 100097.
- [72] C. Pellegrini, A. Marinelli, S. Reiche, Rev. Mod. Phys. 88 (1) (2016), 015006.
- [73] S.C. Mayo, T.J. Davis, T.E. Gureev, P.R. Miller, D. Paganin, A. Pogany, A. W. Stevenson, S.W. Wilkins, Opt. Express 11 (19) (2003) 2289–2302.
- [74] A. Sakdinawat, Y. Liu, Opt. Express 16 (3) (2008) 1559–1564.
- [75] F. Pfeiffer, Nat. Photonics 12 (1) (2018) 9–17.

- [76] D.A. Shapiro, Y.-S. Yu, T. Tyliszczak, J. Cabana, R. Celestre, W. Chao, K. Kaznatcheev, A.L.D. Kilcoyne, F. Maia, S. Marchesini, Y.S. Meng, T. Warwick, L.L. Yang, H.A. Padmore, Nat. Photonics 8 (10) (2014) 765–769.
- [77] C. Donnelly, V. Scagnoli, M. Guizar-Sicairos, M. Holler, F. Wilhelm, F. Guillou, A. Rogalev, C. Detlefs, A. Menzel, J. Raabe, L.J. Heyderman, Phys Rev B 94 (6) (2016), 064421.
- [78] M. Holler, A. Diaz, M. Guizar-Sicairos, P. Karvinen, E. Färm, E. Häkkinen, M. Ritala, A. Menzel, J. Raabe, O. Bunk, Sci. Rep. 4 (1) (2014) 3857.
- [79] X. Shi, P. Fischer, V. Neu, D. Elefant, J.C.T. Lee, D.A. Shapiro, M. Farmand, T. Tyliszczak, H.-W. Shiu, S. Marchesini, S. Roy, S.D. Kevan, Appl. Phys. Lett. 108 (9) (2016), 094103.
- [80] D.J. Chang, D.S. Kim, A. Rana, X. Tian, J. Zhou, P. Ercius, J. Miao, Phys. Rev. B 102 (17) (2020), 174101.
- [81] J. Miao, J. Kirz, D. Sayre, Acta Crystallogr. Sect. D 56 (10) (2000) 1312–1315.
- [82] S. Komineas, N. Papanicolaou, Phys. D-Nonlinear Phenomena 99 (1) (1996) 81–107.
- [83] A.N. Bogdanov, C. Panagopoulos, Phys. Today 73 (3) (2020) 44–49.
- [84] Z. Jiadong, V. Cros, A. Hoffmann, Topology in Magnetism, Springer AG, 2018.
- [85] G. Finocchio, F. Büttner, R. Tomasello, M. Carpentieri, M. Kläui, J. Phys. D Appl. Phys. 49 (42) (2016), 423001.
- [86] F. Büttner, I. Lemesch, G.S.D. Beach, Sci. Rep. 8 (1) (2018) 4464.
- [87] Nicholas Manton, Paul Sutcliffe (Eds.), Topological Solitons, Cambridge University Press, 2004.
- [88] V.M. Kuchkin, B. Barton-Singer, F.N. Rybakov, S. Blügel, B.J. Schroers, N. S. Kiselev, Phys Rev B 102 (14) (2020), 144422.
- [89] J.-S.B. Tai, I.I. Smalyukh, Phys. Rev. Lett. 121 (18) (2018), 187201.
- [90] P. Sutcliffe, Phys. Rev. Lett. 118 (24) (2017), 247203.
- [91] R.A. Battye, P.M. Sutcliffe, Phys. Rev. Lett. 81 (22) (1998) 4798–4801.
- [92] L. Faddeev, A.J. Niemi, Nature 387 (6628) (1997) 58–61.
- [93] E. Feldtkeller, IEEE Trans. Magn. 53 (10) (2017) 1–8.
- [94] W. Kang, Y. Huang, X. Zhang, Y. Zhou, W. Zhao, Proc. IEEE 104 (10) (2016) 2040–2061.
- [95] A. Fert, V. Cros, J. Sampaio, Nat. Nanotechnol. 8 (2013) 152.
- [96] A. Soumyanarayanan, N. Reyren, A. Fert, C. Panagopoulos, Nature 539 (2016) 509.
- [97] N. Nagaosa, Y. Tokura, Nat. Nanotechnol. 8 (2013) 899.
- [98] J. Iwasaki, M. Mochizuki, N. Nagaosa, Nat. Nanotechnol. 8 (2013).
- [99] S. Seki, M. Garst, J. Waizner, R. Takagi, N.D. Khanh, Y. Okamura, K. Kondou, F. Kagawa, Y. Otani, Y. Tokura, Nat. Commun. 11 (1) (2020) 256.
- [100] T. Shinjo, T. Okuno, R. Hassdorf, K. Shigeto, T. Ono, Science 289 (5481) (2000) 930.
- [101] K.Y. Guslienko, V. Novosad, J. Appl. Phys. 96 (8) (2004) 4451–4455.
- [102] K.Y. Guslienko, J. Appl. Phys. 91 (2002).
- [103] M. Schneider, H. Hoffmann, S. Otto, T. Haug, J. Zweck, J. Appl. Phys. 92 (3) (2002) 1466–1472.
- [104] M.Y. Im, P. Fischer, K. Yamada, T. Sato, S. Kasai, Y. Nakatani, T. Ono, Nat. Commun. 3 (2012) 983.
- [105] P. Fischer, M.Y. Im, S. Kasai, K. Yamada, T. Ono, A. Thiaville, Phys. Rev. B 83 (2011) 21.
- [106] M. Weigand, B. Van Waeyenberge, A. Vansteenkiste, M. Curcic, V. Sackmann, H. Stoll, T. Tyliszczak, K. Kaznatcheev, D. Bertwistle, G. Woltersdorf, C.H. Back, G. Schutz, Phys. Rev. Lett. 102 (2009) 7.
- [107] A. Vogel, T. Kamionka, M. Martens, A. Drews, K.W. Chou, T. Tyliszczak, H. Stoll, B. Van Waeyenberge, G. Meier, Phys. Rev. Lett. 106 (2011) 13.
- [108] S. Kasai, P. Fischer, M.Y. Im, K. Yamada, Y. Nakatani, K. Kobayashi, H. Kohno, T. Ono, Phys. Rev. Lett. 101 (23) (2008), 237203.
- [109] M. Curcic, B. Van Waeyenberge, A. Vansteenkiste, M. Weigand, V. Sackmann, H. Stoll, M. Fahrni, T. Tyliszczak, G. Woltersdorf, C.H. Back, G. Schutz, Phys. Rev. Lett. 101 (2008) 19.
- [110] M. Bolte, G. Meier, B. Kruger, A. Drews, R. Eiselt, L. Bocklage, S. Bohlens, T. Tyliszczak, A. Vansteenkiste, B. Van Waeyenberge, K.W. Chou, A. Puzic, H. Stoll, Phys. Rev. Lett. 100 (17) (2008), 176601.
- [111] M. Urbanek, V. Uhlir, C.H. Lambert, J.J. Kan, N. Eibagi, M. Vanatka, L. Flajzman, R. Kalousek, M.Y. Im, P. Fischer, T. Sikola, E.E. Fullerton, Phys Rev B 91 (2015) 9.
- [112] F.U. Stein, L. Bocklage, M. Weigand, G. Meier, Phys. Rev. B 89 (2014) 2.
- [113] M. Noske, A. Gangwar, H. Stoll, M. Kammerer, M. Sroll, G. Dieterle, M. Weigand, M. Fahrni, G. Woltersdorf, C.H. Back, G. Schutz, Phys. Rev. B 90 (2014) 10.
- [114] H.H. Langner, L. Bocklage, T. Matsuyama, G. Meier, Phys. Rev. B 87 (2013) 6.
- [115] M.Y. Im, P. Fischer, H.S. Han, A. Vogel, M.S. Jung, W. Chao, Y.S. Yu, G. Meier, J. I. Hong, K.S. Lee, NPG Asia Mater. 9 (2017).
- [116] A. Vansteenkiste, K.W. Chou, M. Weigand, M. Curcic, V. Sackmann, H. Stoll, T. Tyliszczak, G. Woltersdorf, C.H. Back, G. Schutz, B. Van Waeyenberge, Nat. Phys. 5 (5) (2009) 332–334.
- [117] V. Uhlir, M. Urbanek, L. Hladik, J. Spousta, M.Y. Im, P. Fischer, N. Eibagi, J. J. Kan, E.E. Fullerton, T. Sikola, Nat. Nanotechnol. 8 (5) (2013) 341–346.
- [118] K. Yamada, S. Kasai, Y. Nakatani, K. Kobayashi, H. Kohno, A. Thiaville, T. Ono, Nat. Mater. 6 (4) (2007) 270–273.
- [119] D. Suess, A. Bachleitner-Hofmann, A. Satz, H. Weitensfelder, C. Vogler, F. Bruckner, C. Abert, K. Prügl, J. Zimmer, C. Huber, S. Luber, W. Raberg, T. Schrefl, H. Brückl, Nat. Electron. 1 (6) (2018) 362–370.
- [120] B. Van Waeyenberge, A. Puzic, H. Stoll, K.W. Chou, T. Tyliszczak, R. Hertel, M. Fahrni, H. Brückl, K. Rott, G. Reiss, I. Neudecker, D. Weiss, C.H. Back, G. Schutz, Nature 444 (7118) (2006) 461–464.
- [121] M. Kläui, C.A.F. Vaz, L. Lopez-Diaz, J.A.C. Bland, J. Phys.: Condens. Matter 15 (21) (2003) R985–R1024.
- [122] T. Taniuchi, A. Oshima, H. Akinaga, K. Ono, J. Electron Spectrosc. Relat. Phenom. 144 (2005) 741–744.
- [123] Y.P. Ivanov, R.P. del Real, O. Chubykalo-Fesenko, M. Vázquez, J. Appl. Phys. 115 (6) (2014), 063909.
- [124] S. Velten, R. Streubel, A. Farhan, N. Kent, M.Y. Im, A. Scholl, S. Dhuey, C. Behncke, G. Meier, P. Fischer, Appl. Phys. Lett. 110 (2017) 26.
- [125] K. Nakano, D. Chiba, N. Ohshima, S. Kasai, T. Sato, Y. Nakatani, K. Sekiguchi, K. Kobayashi, T. Ono, Appl. Phys. Lett. 99 (2011) 26.
- [126] H. Jung, Y.-S. Yu, K.-S. Lee, M.-Y. Im, P. Fischer, L. Bocklage, A. Vogel, M. Bolte, G. Meier, S.-K. Kim, Appl. Phys. Lett. 97 (22) (2010), 222502.
- [127] S. Mühlbauer, B. Binz, F. Jonietz, C. Pfleiderer, A. Rosch, A. Neubauer, R. Georgii, P. Böni, Science 323 (5916) (2009) 915.
- [128] X.Z. Yu, N. Kanazawa, Y. Onose, K. Kimoto, W.Z. Zhang, S. Ishiwata, Y. Matsui, Y. Tokura, Nat. Mater. 10 (2) (2011) 106–109.
- [129] W. Jiang, P. Upadhyaya, W. Zhang, G. Yu, M.B. Jungfleisch, F.Y. Fradin, J. E. Pearson, Y. Tservenyak, K.L. Wang, O. Heinonen, S.G.E. te Velthuis, A. Hoffmann, Science 349 (6245) (2015) 283.
- [130] S. Woo, K. Litzius, B. Krüger, M.-Y. Im, L. Caretta, K. Richter, M. Mann, A. Krone, R.M. Reeve, M. Weigand, P. Agrawal, I. Lemesh, M.-A. Mawass, P. Fischer, M. Kläui, G.S.D. Beach, Nat. Mater. 15 (2016) 501.
- [131] C. Moreau-Luchaire, C. Moutafis, N. Reyren, J. Sampaio, C.A.F. Vaz, N. Van Horne, K. Bouzehouane, K. Garcia, C. Deranlot, P. Warnicke, P. Wohlhüter, J. M. George, M. Weigand, J. Raabe, V. Cros, A. Fert, Nat. Nanotechnol. 11 (2016) 444.
- [132] O. Boulle, J. Vogel, H. Yang, S. Pizzini, D. de Souza Chaves, A. Locatelli, T. O. Menteş, A. Sala, L.D. Buda-Prejbeanu, O. Klein, M. Belmeguenai, Y. Roussigné, A. Stashkevich, S.M. Chérif, L. Aballe, M. Foerster, M. Chshiev, S. Auffret, I. M. Miron, G. Gaudin, Nat. Nanotechnol. 11 (2016) 449.
- [133] X. Zhang, Y. Zhou, K. Mee Song, T.-E. Park, J. Xia, M. Ezawa, X. Liu, W. Zhao, G. Zhao, S. Woo, J. Phys.: Condens. Matter 32 (14) (2020), 143001.
- [134] T. Moriya, A. Kawabata, J. Phys. Soc. Jpn. 34 (3) (1973) 639–651.
- [135] A.R. Sandy, Q. Zhang, L.B. Lurio, Annu. Rev. Mater. Res. 48 (1) (2018) 167–190.
- [136] W. Roseker, S.O. Hruszkewycz, F. Lehmkühler, M. Walther, H. Schulthe-Schrepping, S. Lee, T. Osaka, L. Strüder, R. Hartmann, M. Sikorski, S. Song, A. Robert, P.H. Fuoss, M. Sutton, G.B. Stephenson, G. Grüber, Nat. Commun. 9 (1) (2018) 1704.
- [137] M.H. Seaberg, B. Holladay, J.C.T. Lee, M. Sikorski, A.H. Reid, S.A. Montoya, G. L. Dakovski, J.D. Koralek, G. Coslovich, S. Moeller, W.F. Schlötter, R. Streubel, S. D. Kevan, P. Fischer, E.E. Fullerton, J.L. Turner, F.J. Decker, S.K. Sinha, S. Roy, J. J. Turner, Phys. Rev. Lett. 119 (6) (2017), 067403.
- [138] J. Keizer, Phys. Fluids 21 (2) (1978) 198–208.
- [139] D. Sanz-Hernández, R.F. Hamans, J.-W. Liao, A. Welbourne, R. Lavrijsen, A. Fernández-Pacheco, ACS Nano 11 (11) (2017) 11066–11073.
- [140] J.-S.B. Tai, P.J. Ackerman, I.I. Smalyukh, Proc. Natl. Acad. Sci. 115 (5) (2018) 921.
- [141] D. Backes, F. Macià, S. Bonetti, R. Kukreja, H. Ohldag, A.D. Kent, Phys. Rev. Lett. 115 (12) (2015), 127205.
- [142] M.T. Birch, D. Cortés-Ortuño, L.A. Turnbull, M.N. Wilson, F. Groß, N. Träger, A. Laurenson, N. Bukan, S.H. Moody, M. Weigand, G. Schütz, H. Popescu, R. Fan, P. Steadman, J.A.T. Verezinhak, G. Balakrishnan, J.C. Loudon, A.C. Twitchett-Harrison, O. Horváth, H. Fangohr, F.Y. Ogrin, J. Gräfe, P.D. Hatton, Nat. Commun. 11 (1) (2020) 1726.
- [143] X. Xing, Y. Zhou, H.B. Braun, Phys. Rev. Appl. 13 (3) (2020), 034051.
- [144] A.S. Ahmed, J. Rowland, B.D. Esser, S.R. Dunsiger, D.W. McComb, M. Randeria, R.K. Kawakami, Phys. Rev. Mater. 2 (4) (2018), 041401.
- [145] F.S. Zheng, F.N. Rybakov, A.B. Borisov, D.S. Song, S.S. Wang, Z.A. Li, H.F. Du, N. S. Kiselev, J. Caron, A. Kovacs, M.L. Tian, Y.H. Zhang, S. Blugel, R.E. Dunin-Borkowski, Nat. Nanotechnol. 13 (6) (2018) 451.
- [146] K. Ran, Y. Liu, Y. Guang, D.M. Burn, G. van der Laan, T. Hesjedal, H. Du, G. Yu, S. Zhang, Phys. Rev. Lett. 126 (1) (2021), 017204.
- [147] Q. Hu, B. Lyu, J. Tang, L. Kong, H. Du, W. Wang, Appl. Phys. Lett. 118 (2) (2021), 022404.
- [148] A.O. Leonov, K. Inoue, Phys Rev B 98 (5) (2018), 054404.
- [149] C. Donnelly, K.L. Metlov, V. Scagnoli, M. Guizar-Sicairos, M. Holler, N. S. Bingham, J. Raabe, L.J. Heyderman, N.R. Cooper, S. Gliga, Nat. Phys. 17 (3) (2021) 316–321.
- [150] B. Göbel, C.A. Akosa, G. Tata, I. Mertig, Physical Review Research 2 (1) (2020), 013315.
- [151] X.S. Wang, A. Qaiumzadeh, A. Bratas, Phys. Rev. Lett. 123 (14) (2019), 147203.
- [152] Y. Liu, W. Hou, X. Han, J. Zang, Phys. Rev. Lett. 124 (12) (2020), 127204.
- [153] Y. Liu, R.K. Lake, J. Zang, Phys Rev B 98 (17) (2018), 174437.
- [154] P. Sutcliffe, J. Phys. A: Math. Theor. 51 (37) (2018), 375401.
- [155] J.H.C. Whitehead, Proc. Natl. Acad. Sci. 33 (5) (1947) 117.
- [156] A. Bogdanov, A. Hubert, J. Magn. Magn. Mater. 195 (1) (1999) 182–192.
- [157] S. Zhang, F. Kronast, G. van der Laan, T. Hesjedal, Nano Lett. 18 (2) (2018) 1057–1063.
- [158] N. Kent, R. Streubel, C.-H. Lambert, A. Ceballos, S.-G. Je, S. Dhuey, M.-Y. Im, F. Büttner, F. Hellman, S. Salahuddin, P. Fischer, Appl. Phys. Lett. 115 (11) (2019), 112404.
- [159] B.J. McMorrin, J. Unguris, Science 331 (2011) 192.
- [160] Y. Zhu, H. Dürr, Phys. Today 68 (4) (2015) 32–38.
- [161] A.H. Zewail, Annu. Rev. Phys. Chem. 57 (1) (2006) 65–103.
- [162] A. Feist, K.E. Echternkamp, J. Schauss, S.V. Yalunin, S. Schäfer, C. Ropers, Nature 521 (7551) (2015) 200–203.